Carrier escape from ground state and non-zero resonance frequency at low bias powers for semiconductor quantum-dot lasers

C. Wang[a*], F. Grillot[a,b] and J. Even[a]

[a]Université Européenne de Bretagne, INSA, CNRS FOTON, 20 avenue des buttes de Coesmes, 35708 Rennes Cedex 7, France

[b]Telecom Paristech, Ecole Nationale Supérieure des Télécommunications, CNRS LTCI, 46 rue Barrault, 75013 Paris, France

ABSTRACT

The three-dimensional confinement of electrons and holes in the semiconductor quantum dot (QD) structure profoundly changes its density of states compared to the bulk semiconductor or the thin-film quantum well (QW) structure. The aim of this paper is to theoretically investigate the microwave properties of InAs/InP(311B) QD lasers. A new expression of the modulation transfer function is derived for the analysis of QD laser modulation properties based on a set of four rate equations. Analytical calculations point out that carrier escape from ground state (GS) to excited state (ES) induces a non-zero resonance frequency at low bias powers. Calculations also show that the carrier escape leads to a larger damping factor offset as compared to conventional QW lasers. These results are of prime importance for a better understanding of the carrier dynamics in QD lasers as well as for further optimization of low cost sources for optical telecommunications.

Keywords: laser, quantum dot, semiconductor, modulation response

1. INTRODUCTION

Self-organised quantum dot (QD) lasers are promising laser sources for optical fibre communications because of their attractive characteristics, such as low threshold current density [1], high differential gain [2], high bandwidth [3,4] and reduced frequency chirp [5,6]. QD lasers are expected to be alternatives of the quantum well (QW) counterparts for optical telecommunications. More particularly, Directly Modulated Lasers (DML) can play a major role in the next-generation telecommunication links for cooler-less and isolator-free applications. However, although QD DMLs are compact, cheap and easy to fabricate, the maximum modulation bandwidth remains still limited to 10-12 GHz [7,8] at wavelengths in the 1300-1500 nm bands namely much below than the best values reported for QW lasers. The modulation bandwidth is known to be strongly dependent on both the resonance frequency as well as on the damping factor. In semiconductor lasers, the resonance frequency is limited by the maximum modal gain and by nonlinear effects [9]. In particular, QD lasers are commonly observed to exhibit a stronger damping compared to their QW counterparts [10,11,12], which limits the bandwidth efficiency. Although the underlying physical mechanisms are still under investigation, carrier capture dynamics [13,14,15], Coulomb interaction [12] and gain compression [11] have been proposed to the origins. The conventional modulation transfer function usually derived from the two standard rate equations is an efficient tool for the analysis of QW laser modulation characteristics [9]. However, in the case of QD lasers, a more sophisticated model is required. This paper aims to clarify the origins of the limited modulation bandwidth of InAs/InP(311B) QD lasers, and then to figure out various ways of optimization to match the modulation properties with the network requirement [17]. One theoretical approach to study QD laser dynamics is to simulate the modulation properties numerically based on a set of rate equations [12]. In order to identify the key-parameters controlling the carrier dynamics as well as the QD laser modulation response, an analytical approach is conducted. Following a similar approach, Sugawara et. al proposed an empirical expression to fit the experimental modulation response [16]. Let us also note that Fiore et. al also developed an indirect approach to recast the set of complex QD rate equations into the standard QW rate equations [8]. In this paper, taking into account the influences of both the wetting layer (WL) and the excited state (ES), a new analytical modulation transfer function is proposed based on a set of four rate differential equations [18]. Definitions of relaxation resonance frequency and damping factor are recasted as well.

* cheng.wang@insa-rennes.fr; phone +33 223238464;

The analytical analysis shows that carrier escape from GS to ES is responsible for the commonly observed strong damping of QD lasers, and leads to a non-zero resonance frequency at low bias powers. These results are significant for a better understanding of carrier dynamics of QD lasers and point to possible routes for the improvement of QD laser dynamic properties.

2. STEADY-STATE PROPERTIES AND TURN-ON DELAY PROPERTIES

2.1 Numerical model description

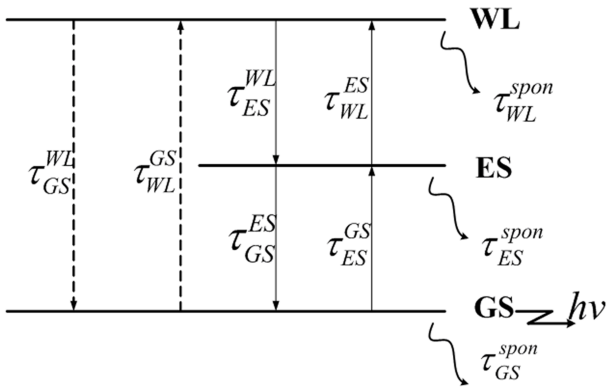

Figure 1. Illustration of carrier dynamics model including a direct relaxation channel (dash lines)

Figure 1 shows the schematic of the carrier dynamics for the InAs/InP(311B) QD laser under study[18]. The model holds under the assumption that there is only one QD ensemble in which nanostructures are interconnected by a wetting layer (WL). The inhomogeneous broadening related to the QD size dispersion is not taken into account. In this ensemble, two energy levels are assumed: a two-fold degenerated GS and a four-fold degenerated excited state (ES). Electrons (e) and holes (h) are considered to be captured and emitted in pairs (eh). Carriers are supposed to be injected directly from the metallic contacts into the WL levels. Then, carriers are either captured into ES within time τ_{ES}^{WL} or directly into the GS within time τ_{GS}^{WL}. Once in the ES level, carriers can also relax to GS within time τ_{GS}^{ES}. On the other hand, the eh-pairs recombine spontaneously or escape from GS and ES within times τ_{ES}^{GS}, τ_{WL}^{GS} and τ_{WL}^{ES}. The eh-pair escape times have been derived for both the ES and GS carriers assuming the system in the quasi-thermal equilibrium (Fermi distribution) without external excitation [19].

Following the sketch of figure 1, the four rate equations on carrier and photon number are as follows:

$$\frac{dN_{WL}}{dt} = \frac{I}{q} + \frac{N_{ES}}{\tau_{WL}^{ES}} - \frac{N_{WL}}{\tau_{ES}^{WL}} f_{ES} - \frac{N_{WL}}{\tau_{GS}^{WL}} f_{GS} - \frac{N_{WL}}{\tau_{WL}^{spon}} + \frac{N_{GS}}{\tau_{WL}^{GS}} \tag{1}$$

$$\frac{dN_{ES}}{dt} = \frac{N_{WL}}{\tau_{ES}^{WL}} f_{ES} + \frac{N_{GS}}{\tau_{ES}^{GS}} f_{ES} - \frac{N_{ES}}{\tau_{WL}^{ES}} - \frac{N_{ES}}{\tau_{GS}^{ES}} f_{GS} - \frac{N_{ES}}{\tau_{ES}^{spon}} \tag{2}$$

$$\frac{dN_{GS}}{dt} = \frac{N_{WL}}{\tau_{GS}^{WL}} f_{GS} + \frac{N_{ES}}{\tau_{GS}^{ES}} f_{GS} - \frac{N_{GS}}{\tau_{ES}^{GS}} f_{ES} - \frac{N_{GS}}{\tau_{GS}^{spon}} - g_{GS} v_g S_{GS} - \frac{N_{GS}}{\tau_{WL}^{GS}} \tag{3}$$

$$\frac{dS_{GS}}{dt} = \Gamma_p g_{GS} v_g S_{GS} - \frac{S_{GS}}{\tau_P} + \beta_{SP} \frac{N_{GS}}{\tau_{GS}^{spon}} \tag{4}$$

where $N_{WL,ES,GS}$ are carrier numbers in WL, ES, GS and S_{GS} is photon number. $\tau_{WL,ES,GS}^{spon}$ are spontaneous emission times, β_{SP} is spontaneous emission factor and Γ_p is optical confinement factor. v_g is the group velocity and τ_p is photon lifetime.

The GS gain is described as follows:

$$g_{GS} = a_{GS} N_B \left(\frac{N_{GS}}{N_B} - 1 \right) \tag{5}$$

where a_{GS} is the differential gain and N_B is the total QD number.

The probabilities $f_{GS,ES}$ to find an empty carrier state in GS and ES are given by:

$$f_{GS} = 1 - \frac{N_{GS}}{2N_B}; \quad f_{ES} = 1 - \frac{N_{ES}}{4N_B} \tag{6}$$

Since the carrier escape from GS to WL has been demonstrated to have little effects on laser properties [18], the N_{GS} / τ_{WL}^{GS} term in Eq. (1) and Eq. (3) can be neglected.

2.2 Steady-state properties and turn-on delay properties

Steady-state properties as well as turn-on delay properties are studied by numerically solving the four rate equation model. The capture time τ_{ES}^{WL} and relaxation time τ_{GS}^{ES} are chosen based on the time resolved photoluminescence experiment [20]. The direct carrier capture time from WL to GS τ_{GS}^{WL} is observed to be larger than the capture time τ_{ES}^{WL} in low excitation regime [21], while under strong excitation τ_{GS}^{WL} becomes as short as τ_{ES}^{WL}, namely it can be assumed $\tau_{GS}^{WL} \approx \tau_{ES}^{WL}$ [20]. In our calculation, we take $\tau_{GS}^{WL} = 1.5\tau_{ES}^{WL}$ and the differential gain $a_{GS} = 0.5\times10^{-14}$ cm^2. All laser parameters used in the simulations are summarized in table 1.

Table 1. The QD material parameters and the laser parameters

QD material parameters		Laser parameters	
WL energy:	E_{WL}=0.97 eV	Active region length:	L=0.11 cm
ES energy:	E_{ES}=0.87 eV	Active region width:	W=3×10^{-4} cm
GS energy:	E_{GS}=0.82 eV	Number of QD layers:	N=5
Capture time from WL to ES:	τ_{ES}^{WL} =25.1 ps	QD density:	N_D=5×10^{10} cm^{-2}
Relaxation time from ES to GS:	τ_{GS}^{ES} = 11.6 ps	Optical confinement factor:	Γ_p =0.06
Spontaneous time of WL and ES:	$\tau_{WL}^{spon} = \tau_{ES}^{spon}$ =500 ps	Spontaneous emission factor:	β_{SP} =1× 10^{-4}
Spontaneous time of GS:	τ_{GS}^{spon} =1200 ps	Internal modal loss:	α_i =6 cm^{-1}
Refractive index:	n_r=3.27	Mirror reflectivity:	R_1=R_2=0.3

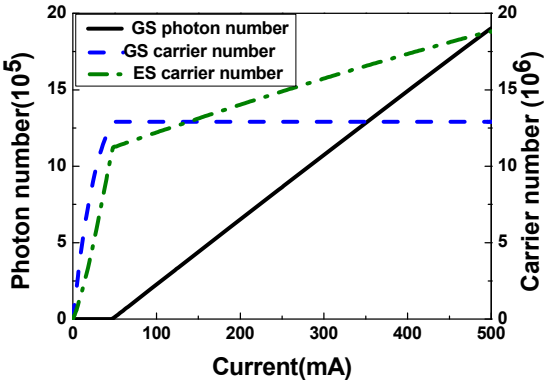

Figure 2. Calculated photon number and carrier number as a function of injected current.

As an example, steady-state properties of the InAs/InP (311B) QD laser are shown in figure 2. With the increase of the pump current, both the carrier populations in the GS and the ES are enhanced. Then, for an injected current larger than 48 mA, the GS population gets clamped which leads to the occurrence of the GS lasing emission (while the ES population continues increasing with a reduced slope efficiency). Figure 3 also presents the transient responses of GS lasing at several current injections. With the increase of the injected current, simulations also point out that the delay time becomes shorter which means that the carrier lifetime is lowered [22]. Both the oscillation frequency and the damping factor get larger with the pump current. For instance, the oscillation frequencies at 75 mA, 100 mA and 200 mA are 1.94GHz, 2.64 GHz and 3.52 GHz, respectively. The relaxation oscillation cannot be distinguished at 300 mA due to the strong damping of relaxation oscillations.

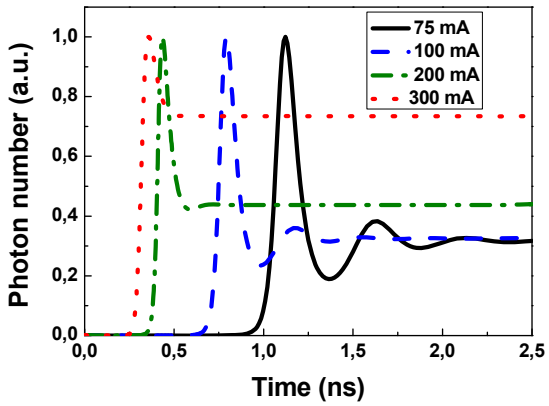

Figure 3. Turn-on delay of the GS lasing at various current injection levels.

3. SMALL-SIGNAL ANALYSIS OF INTENSITY MODULATION RESPONSE

3.1 Analytical derivations

Based on the set of rate equations (1-4) and considering $I, N_{WL}, N_{ES}, N_{GS}, S_{GS}$ as well as g_{GS} as dynamic variables, we can derive the differential rate equations on carrier and photon density:

$$\frac{d}{dt}\begin{bmatrix} dN_{WL} \\ dN_{ES} \\ dN_{GS} \\ dS_{GS} \end{bmatrix} = \begin{bmatrix} -\gamma_{11} & \gamma_{12} & 0 & 0 \\ \gamma_{21} & -\gamma_{22} & \gamma_{23} & 0 \\ \gamma_{31} & \gamma_{32} & -\gamma_{33} & \gamma_{34} \\ 0 & 0 & \gamma_{43} & -\gamma_{44} \end{bmatrix}\begin{bmatrix} dN_{WL} \\ dN_{ES} \\ dN_{GS} \\ dS_{GS} \end{bmatrix} + \frac{dI}{qV}\begin{bmatrix} 1 \\ 0 \\ 0 \\ 0 \end{bmatrix} \tag{7}$$

where

$$\begin{aligned}
&\gamma_{11} = \frac{f_{ES}}{\tau_{ES}^{WL}} + \frac{f_{GS}}{\tau_{GS}^{WL}} + \frac{1}{\tau_{WL}^{spon}};\quad \gamma_{12} = \frac{1}{\tau_{WL}^{ES}};\quad \gamma_{21} = \frac{f_{ES}}{\tau_{ES}^{WL}} \\
&\gamma_{22} = \frac{f_{GS}}{\tau_{GS}^{ES}} + \frac{1}{\tau_{WL}^{ES}} + \frac{1}{\tau_{ES}^{spon}} \\
&\gamma_{23} = \frac{f_{ES}}{\tau_{ES}^{GS}};\quad \gamma_{31} = \frac{f_{GS}}{\tau_{GS}^{WL}};\quad \gamma_{32} = \frac{f_{GS}}{\tau_{GS}^{ES}} \\
&\gamma_{33} = \frac{f_{ES}}{\tau_{ES}^{GS}} + \frac{1}{\tau_{GS}^{spon}} + v_g a_{GS} S_{GS};\quad \gamma_{34} = v_g a_{GS}^p S_{GS} - v_g g_{GS} \\
&\gamma_{43} = \frac{\Gamma_p \beta_{SP}}{\tau_{GS}^{spon}} + \Gamma_p v_g a_{GS} S_{GS};\quad \gamma_{44} = \Gamma_p v_g a_{GS}^p S_{GS} - \Gamma_p v_g g_{GS} + \frac{1}{\tau_p}
\end{aligned} \tag{8}$$

In Eqs. (8), the gain variation is expressed as

$$dg_{GS} = a_{GS} dN_{GS} - a_{GS}^p dS_{GS} \tag{9}$$

with $a_{GS}^p = -\partial g_{GS} / \partial S_{GS}$ a coefficient taking into account the gain compression effects. Applying a small-signal analysis to the differential rate equations allows extracting a new expression of the QD laser's modulation response:

$$H(w) \equiv \frac{R_0}{R_0 + jwR_1 - w^2 R_2 - jw^3 R_3 + w^4} \tag{10}$$

The four parameters R_0, R_1, R_2 and R_3 characterizing $H(w)$ are given by:

$$\begin{aligned} R_0 &= w_R^2(\gamma_{11}\gamma_{22}-\gamma_{12}\gamma_{21})-\gamma_{23}\gamma_{44}(\gamma_{31}\gamma_{12}+\gamma_{11}\gamma_{32}) \\ R_1 &= w_R^2(\gamma_{11}+\gamma_{22})+\Gamma(\gamma_{11}\gamma_{22}-\gamma_{12}\gamma_{21})-\gamma_{23}\gamma_{32}(\gamma_{11}+\gamma_{44})-\gamma_{31}\gamma_{12}\gamma_{23} \\ R_2 &= w_R^2+\Gamma(\gamma_{11}+\gamma_{22})+(\gamma_{11}\gamma_{22}-\gamma_{12}\gamma_{21})-\gamma_{23}\gamma_{32} \\ R_3 &= \Gamma+(\gamma_{11}+\gamma_{22}) \end{aligned} \tag{11}$$

And the improved relaxation resonance frequency w_R and damping factor Γ are defined as

$$w_R^2 = \gamma_{33}\gamma_{44}-\gamma_{34}\gamma_{43} \tag{12}$$

$$\Gamma = \gamma_{33}+\gamma_{44} \tag{13}$$

Eq. (12) and Eq. (13) constitute new analytical relationships giving the resonance frequency and the damping factor of a QD laser. It is important to note that these improved definitions differ from those related to QW lasers [9]. For instance, because of the QD structure, w_R^2 and Γ contain an additional term f_{ES}/τ_{ES}^{GS} describing the carrier escape from the GS to the ES.

Well beyond the laser's threshold, the resonance frequency can be reduced to

$$w_R^2 \approx v_g S_{GS} a_{GS}/\tau_p \tag{14}$$

Eq. (14) constitutes the very well-known expression pointing out that the resonance frequency can be enhanced by increasing the photon density, the differential gain, or by decreasing photon lifetime namely by decreasing the cavity length.

Employing this simplified definition of w_R^2 and rewrite the damping factor:

$$\Gamma = Kf_R^2+\Gamma_N \tag{15}$$

where the so-called K-factor is as follows:

$$K = 4\pi^2\tau_p\left(1+\frac{\Gamma a_{GS}^p}{a_{GS}}\right) \tag{16}$$

and the offset is:

$$\Gamma_N = \frac{f_{ES}}{\tau_{ES}^{GS}}+\frac{1}{\tau_{GS}^{spon}}+\frac{\Gamma_p\beta_{SP}N_{GS}}{\tau_{GS}^{spon}S_{GS}} \tag{17}$$

The expression of K-factor is found to be the same as of the conventional one for QW lasers. The term f_{ES}/τ_{ES}^{GS} in Γ_N dominates in the offset and is comparable to Kf_R^2 even at high bias powers, so the offset can not be neglected.

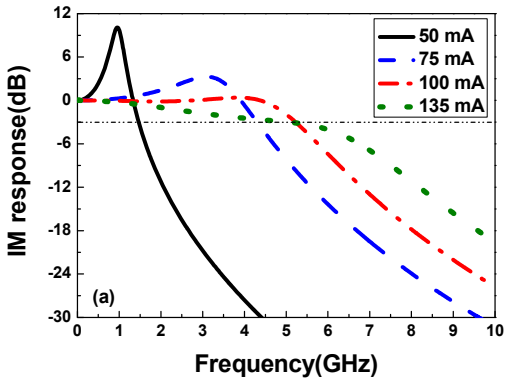

Figure 4. Intensity modulation response at several injected currents.

Based on the steady-state results obtained in the previous section, the modulation responses are calculated from Eq. (10) for various current levels. Figure 4 shows the numerical results for both the relaxation frequency and the damping factor, and they both increase for higher pump currents. At high pumping levels, the resonance peak is even suppressed which leads to a relatively flat modulation response. At a current injection of around 135 mA, the modulation bandwidth reaches the maximum value ~5.5 GHz, which is in good agreement with the commonly measured values [23,24,25].

3.2 Comparison to experimental results

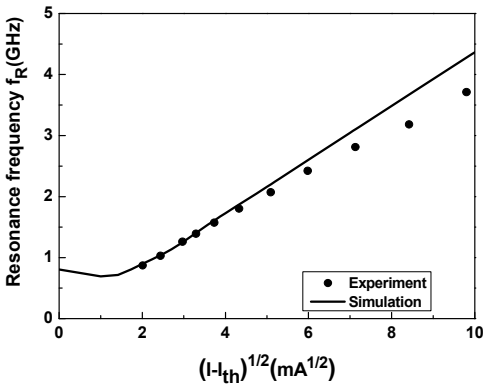

Figure 5. The resonance frequency as a function of the normalized current. Dots are the experimental results from [17] while the solid line corresponds to calculations.

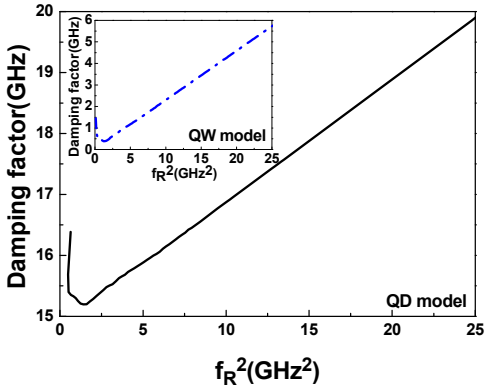

Figure 6. Comparisons of damping factor from our improved QD model and that from the QW model (inset).

In order to validate the numerical results, a comparison with experiments is now conducted. The device under study is a InAs/InP(311B) QD laser [17], where the heterostructure is grown by MBE on a (311)B oriented InP substrate and it has as-cleaved facets. The active region consists of 5 QD layers, and the dot density is ~10^{11}cm^2 [26]. The length and width of the ridge wave-guide FP laser are 1.1 mm and 3×10^{-3} mm, respectively. Experiments show a GS lasing peak at 1.52 μm at room temperature in continuous wave (cw) operation and the photon lifetime is measured to be 5.8 ps. In this section, we use the new analytical transfer function Eq. (10) to simulate the laser modulation performance. In the calculations, the differential gain a_{GS} is the only fitting parameter, which is adjusted to 0.25×10^{-14} cm^2. All the other parameters are set to the experimental values.

Figure 5 shows that the resonance frequency f_R as a function of the normalized current $(I-I_{th})^{1/2}$. Numerical results (solid line) obtained from Eq. (10) show a relative good agreement with the experimental results (dots). However, at large current injections, the calculated resonance frequency is higher than the experimental result. Such a discrepancy can be attributed to the gain compression effects which has been zeroed (a_{GS}^{p} =0) in the calculations. Figure 5 also points out that the carrier escape from the GS to the ES induces a non-zero resonance frequency around 1 GHz at low bias powers. This resonance frequency offset is larger than the one due to spontaneous emission only in QW lasers [9]. Based on Eq. (12), the larger τ_{ES}^{GS} the smaller the frequency offset at low bias powers.

Figure 6 shows the evolution of damping factor Γ as a function of resonance frequency f_R^2. Through linear fitting of the

plot, the relation of QD laser is obtained as $\Gamma = 0.20 f_R^2 + 14.9$ (GHz), in comparison with the result from conventional QW model (inset): $\Gamma = 0.23 f_R^2 + 0.066$ (GHz). The two K-factors are nearly the same ~0.2 ns, which is 3 times smaller than the experimental value 0.6 ns [17]. Again, this discrepancy can be attributed to the fact that the simulation does not take into account the gain saturation effects. Further studies will investigate the influence of Γa_{GS}^p which is comparable to the differential gain a_{GS} [9]. Simulations demonstrate that the offset of damping factor is much larger for QD lasers than that from the QW model. According to Eq. (15), the large damping factor offset Γ_N is attributed to the carrier escape from GS to ES (f_{ES} / τ_{ES}^{GS}). Because the carrier escape time τ_{ES}^{GS} is linked to the carrier relaxation time τ_{GS}^{ES} which is typically in the range of 1—100 ps, so τ_{GS}^{ES} plays a major role in the determination of the offset value to the damping factor. This large offset value can well confirm the commonly observed strong damping in QD lasers [10,12], which also partially explains the QD laser's insensitivity to external perturbations. The deviation from linearity at low relaxation resonance frequency is because of the spontaneous emission term $(\Gamma_p \beta_{SP} N_{GS}) / (\tau_{GS}^{spon} S_{GS})$ in the damping factor expression. This phenomenon has been observed in InGaAsP bulk lasers via a parasitic-free optical modulation technique [27].

4. CONCLUSION

A new analytical expression of the modulation response has been derived for QD lasers, Calculations take into account the influences of various quantum states such as the wetting layer (WL), the first excited states (ES) and the ground state (GS). Based on the analytical derivations, definitions of resonance frequency and damping factor have been recasted. At low bias powers, carrier escape from GS to ES gives rise to a non-zero resonance frequency associated with a strong damping rate. These results are of first importance for a better understanding of the carrier dynamics in QD lasers for high-speed applications, and point to possible routes for the improvement of QD laser dynamics as well.

ACKNOWLEDGMENTS

The authors are grateful to the TELDOT project from the French national initiative ANR and to Rennes Metropole for financial supports.

REFERENCES

[1] Liu, G. T., Stintz, A., Li, H., Malloy, K. J., and Lester, L. F. ,"Extremely low room-temperature threshold current density diode lasers using InAs dots in In Ga As quantum well," Electron. Lett. 35(14), 1163–1165 (1999).
[2] Bimberg, D., Kirstaedter, N., Ledentsov, N. N., Alferov, Z. I., Kopev, P. S., and Ustinov, V. M., "InGaAs-GaAs quantum-dot lasers," IEEE J. Sel. Topics Quantum Electron. 3(2), 196–205 (1997).
[3] Mi, Z., Bhattacharya, P., and Fathpour, S., "High-speed 1.3 μm tunnel injection quantum-dot lasers," Appl. Phys. Lett. 86, 153109 (2005).
[4] Kuntz, M., Fiol, G., Lammlin, M., Schubert, C., Kovsh, A. R., Jacob, A., Umbach, A., and Bimberg, D., "10Gbit/s data modulation using 1.3μm InGaAs quantum dot lasers," Electron. Lett. 41, 244-245 (2005).
[5] Saito, H., Nishi, K., Kamei, A., and Sugou, S., "Low chirp observed in directly modulated quantum dot lasers," IEEE Phot. Tech. Lett. 12(10), 1298-1300 (2000).
[6] Ghosh, S., Pradhan, S., and Bhattacharya, P., "Dynamic characteristics of high-speed In0.4Ga0.6As/GaAs self-organized quantum dot lasers at room temperature," Appl. Phys. Lett. 81, 3055-3057 (2002).
[7] Grillot, F., Dagens, B., Provost, J.G., Su, H., and Lester, L. F., "Gain compression and above-threshold linewidth enhancement factor in 1.3μm InAs-GaAs quantum dot lasers," IEEE Journal of Quantum Electronics, 44(10), 946-951 (2008).
[8] Fiore, A., and Markus, A., "Differential gain and gain compression in quantum-dot lasers," IEEE Journal of Quantum Electronics, 43(3), 287-294 (2007).
[9] Coldren, L. A., and Corzine, S. W., [Diode Lasers and Photonic Integrated Circuits], John Wiley & Sons, New York, 195-204 (1995).

[10] Kuntz, M., Ledentsov, N. N., Bimberg, D., Kovsh, A. R., Ustinov, V. M., "Spectrotemporal response of 1.3 μm quantum-dot lasers," Appl. Phys. Lett. 81(20), 3846-3848 (2002).
[11] O'Brien, D., Hegarty, S.P., Huyet, G., McInerney, J.G., Kettler, Laemmlin, T., Bimberg, D., Ustinov, V.M., Zhukov, A.E., Mikhrin, A.R., and Kovsh, A.R., "Feedback sensitivity of 1.3 μm InAs/GaAs quantum dot laser," Electron. Lett. 39 (25), 1819–1820 (2003).
[12] Malic, E., Ahn, K.J., Bormann, M. J., Hovel, P., Scholl, E., Knorr, A., Kuntz, M., and Bimberg, D., "Theory of relaxation oscillations in semiconductor quantum dot lasers," Appl. Phys. Lett. 89, 101107 (2006)
[13] Klotzkin, D., Kamath, K., and Bhattacharya, P., "Quantum capture times at room temperature in high-speed InGa As–GaAs self-organized quantum-dot lasers," IEEE Phot. Tech. Lett. 9(10), 1301-1303 (1997)
[14] Ishida, M., Hatori, N., Akiyama, T., Otsubo, K., Nakata, Y., Ebe, H., Sugawara, M., and Arakawa, Y., "Photon lifetime dependence of modulation efficiency and K factor in 1.3 μm self-assembled InAs/GaAs quantum-dot lasers: Impact of capture time and maximum modal gain on modulation bandwidth," Appl. Phys. Lett. 85, 4145-4147 (2004)
[15] O'Brien, D., Hegarty, S.P.,Huyet, G., and Uskov, A.V., "Sensitivity of quantum dot semiconductor lasers to optical feedback, " Opt. Lett. 29, 1072-1074 (2004).
[16] Sugawara, M. [Self-Assembled InGaAs-GaAs Quatum Dots], Academic press, San Diego, CA, (1999).
[17] Martinez, A., Merghem, K., Bouchoule, S., Moreau, G., Ramdane, A., Provost, J. G., Alexandre, F., Grillot, F., Dehaese, O., Piron, R. and Loualiche, S., "Dynamic properties of InAs/InP(311B) quantum dot Fabry-Perot lasers emitting at 1.52-μm", Appl. Phys. Lett., 93, 021101 (2008).
[18] Veselinov, K., Grillot, F., Cornet, C., Even, J., Bekiarski, A., Gioannini, M. and Loualiche, S., "Analysis of the Double Laser Emission Occurring in 1.55-μm InAs–InP (113)B Quantum-Dot Lasers," IEEE Journal of Quantum Electron., 43(9), 810-816 (2007).
[19] Grillot, F., Veselinov, K., Gioannini, M., Montrosset, I., Even, J., Piron, R., Homeyer, E., and Loualiche, S., "Spectral analysis of 1.55 μm InAs–InP(113)B quantum-dot lasers based on a multipopulation rate equations model," IEEE Journal of Quantum Electron., 45(7), 872-878 (2009).
[20] Miska, P. , Even, J., Dehaese, O., and Marie, X., "Carrier relaxation dynamics in InAs/InP quantum dots," Appl. Phys. Lett. 92, 191103 (2008).
[21] Bockelmann, U., and Egeler, T., "Electron relaxation in quantum dots by means of Auger processes," Phys. Rev. B, Condens. Phys. 46, 15574-15577 (1992).
[22] Agrawal, G. P., and Dutta, N. K., [Long Wavelength Semiconductor Lasers] , Van Nostrand Reinhold, New York, 240-244 (1986).
[23] Sugawara, M., Hatori, N., Ishida, M., Ebe, H., and Arakawa, Y., "Recent progress in self-assembled quantum-dot optical devices for optical telecommunication: Temperature-insensitive 10 Gbs^{-1} directly modulated lasers and 40 Gbs^{-1}signal-regenerative amplifiers, " J. Phys. D, Appl. Phys. 38 (13), 2126–2134 (2005).
[24] Bhattacharya, P., and Mi, Z., "Quantum-dot optoelectronic devices," Proc. IEEE 95 (9),1723-1740 (2007)
[25] Krebs, R., Klopf, F., Rennon, S., Reithmaier, J.P., and Forchel, A., "High frequency characteristics of InAs/ GalnAs quantum dot distributed feedback lasers emitting at 1.3 μm," Electron. Lett. 37 (20), 1223-1225 (2001)
[26] Massé, N. F., Homeyer, E., Adams, A. R., Sweeney, S. J., Dehaese, O., Piron, R., Grillot F., Loualiche, S., "Temperature and pressure dependence of the recombination processes in 1.5μm InAs/InP (311)B quantum dot lasers, " Appl. Phys. Lett. 91, 131113-131115 (2007).
[27] Su, C. B., Eom, J., William, C., Rideout, C., Lange, H., Kim, C. B., Lauer, R. B., and Lacourse, J. S., "Characterization of the Dynamics of Semiconductor Lasers using Optical Modulation, " IEEE Journal of Quantum Electron., 28(1), 118-127 (1992).